

1

Physics and fate of jet related emission line regions

Martin G. H. Krause

Max-Planck-Institut für extraterrestrische Physik,
Giessenbachstrae, 85748 Garching, Germany and

Universitätssternwarte München,

Ludwig-Maximilians-Universität, Scheinerstr. 1,
81679 München, Germany

Volker Gaibler

Max-Planck-Institut für extraterrestrische Physik,
Giessenbachstrae, 85748 Garching, Germany

1.1 Introduction

At redshifts above $z \gtrsim 0.5$ extragalactic jet sources are commonly associated with extended emission line regions (for a review see 19; 21). The most prominent emission line is the hydrogen Lyman α line, but other typical nebular emission lines have also been found. These regions are up to 100 kpc in extent, anisotropic and preferentially aligned with the radio jets (*alignment effect*). Their properties correlate with the ones of the radio jets: Smaller radio jets (< 100 kpc) have more extended emission line regions with larger velocity widths (1000 km s^{-1}) that are predominantly shock ionised, as diagnosed from their emission line ratios. Larger radio jets (> 100 kpc) have emission line regions even smaller than 100 kpc. Their turbulent velocities are typically about 500 km/s and the dominant excitation mechanism is photo-ionisation.

The physical function of these emission line regions can be compared to a detector in a particle physics experiment: In both cases a beam of high energy particles hits a target. Analysis of the interactions in the surrounding detector, or in astrophysics the emission line gas, provides information about the physical processes of interest. For the astrophysical jets, the information one would like to obtain from such analysis concerns two traditionally separated branches of astrophysics:

The considerable energy release that may be associated with the jet phenomenon is received by a large reservoir of gas surrounding the host galaxy. Compression and heating of that gas may influence the star formation his-

tory of the host galaxy, in both ways, triggering and suppression of star formation (1; 5; 25). Also, the jets transfer a bulk momentum to the emission line gas surrounding the galaxy. The observed speeds in the emission line gas are typically of order the escape velocity of the host system (23). This may lead to observable effects in the spectral energy distribution of that galaxy at later times (e.g. 25), and might even be part of the answer of the question, why the mass of the supermassive black holes correlate with properties of the host galaxies (e.g. 10).

The other branch is the physics of active galactic nuclei. Extragalactic jets originate in the immediate vicinity of super-massive black holes. How the jet production is really happening is not entirely clear yet, partly because the horizon scale, which is the characteristic size of a black hole, cannot be resolved by any instrument in any object. Also, an adequate treatment of the Kerr metric, which permits angular momentum exchange in both ways between the black hole and the plasma in the surrounding accretion disk via magnetic torques, is still a challenge to current magnetohydrodynamic (MHD) studies of accretion physics, though progress is being made (11). Within the theory of General Relativity, black holes have, in principal three basic properties: mass, angular momentum and charge. As usual in astrophysics, the charge is assumed to be negligible. Black hole masses are in general well measured. Because the horizon scale is proportional to the mass, the mass, together with the accretion rate, sets the scale for the overall energy output. Jet production might be coupled to the black hole's angular momentum and magnetosphere. The latter may be considerably different for different environmental conditions, especially accretion rates. Some black holes develop a strong quasar activity having at the same time powerful jets, while some do not. Common sense suggests that, since masses and accretion rates do not seem to make a difference, the black hole's angular momentum, together with the magnetosphere, might be the decisive point (e.g. 3; 4; 20). important evidence for or against this hypothesis might in future come from correlating reliable measurements of black hole spins and jet powers. Black hole spins have been measured from relativistically deformed iron lines of near horizon material (e.g. 22; 26, and references therein). The values found include rapidly spinning black holes close to the limit allowed by the Kerr metric (cosmic censorship conjecture). Jet powers have so far been constrained from the interaction with the ambient gas, mainly from X-ray data (e.g. 15; 2), but also first attempts have been made to use the energy in the emission line gas for this (23).

Jet beams are nearly dissipationless, and transport various kinds of information to large scales, where they might in principle be deduced from

careful observation and analysis of their interaction with the environment: the jet’s power, mass flux, particle composition, net electric current, and also the sense of the toroidal as well as the direction of the axial magnetic field should be conserved along the jet beam. Extended emission line regions may in principle serve as calorimeters. Indeed, the emission line power is correlated with the radio power (e.g. 19). If shock ionisation is firmly deduced from the emission line ratios, we may conclude that the power source of the radiation is the jet. Also, the kinetic energy in the emission line gas, which can now be quite accurately determined from integral field spectroscopy is a lower bound for the energy released by the jet. For two powerful radio galaxies at a redshift of about two, (23) give the observed radio power, power in the $H\alpha$ line and the power required to account for the kinetic energy in the emission line gas: Each value is a few times 10^{45} erg/s.

Here, we present hydrodynamics (HD) and magnetohydrodynamics simulations of the interaction of powerful radio jets with their environment with an emphasis on the cold gas ($T < 10^6\text{K}$), which includes the emission line gas. We constrain the locus of the emission line regions as well as the fraction of the jet power they receive by global simulations in section 1.2. We present local box simulations of the multi-phase turbulence on small scales in section 1.3, which can be used to infer properties of the emission line gas like kinematics or condensation rate from the hot gas entrained into the radio cocoons. We discuss our results and present the conclusions in section 1.4

1.2 Global jet simulations

We have recently carried out a parameter study of global jet simulations with the MHD code *NIRVANA* (27; 8; 9). The jets are injected with Mach 6 into a constant ambient density environment. Here, we use the results for the simulation with a density ratio of 10^{-3} . We use an innovative magnetic field configuration: a helical magnetic field constrained to the jet material, which is almost zero in the ambient medium. The global morphology of this simulations is shown in Fig. 1.1. The narrow jet beams propagate essentially undisturbed from the centre of the image out to the edges of the low density cocoon. The supersonic beams are shocked there at the so-called Mach disk. The kinetic energy is transferred into thermal and produces the hot spots there. Because of the large density contrast, the excess pressure of the hot spots drives comparatively slow bow shocks into the surrounding gas, which may be seen in Fig. 1.1 as an elliptical structure surrounding the source. Because of the slow bow shock expansion, the jet plasma has to flow

backwards from the hot spots. At the same time it expands sideways till it reaches pressure equilibrium with the surrounding layer of shocked ambient gas. The resulting width of the low density cocoon is anti-correlated to the jet/ambient density ratio. The large cocoon widths observed in extragalactic radio jets usually require light jets, often the inferred jet density is three to four orders of magnitude below the ambient density. The simulations have shown that very light jets produce a thick layer of shocked ambient gas, and weak bow shocks. Where the bow shock can be identified in X-ray data, both predictions are confirmed (e.g. 24). The contact surface between the low density cocoon and the shocked ambient gas layer, though partly stabilised by magnetic fields, is ragged by Kelvin-Helmholtz instabilities. Here, the ambient gas is entrained into the radio cocoon, where it is accelerated by the turbulent cocoon motions. Turbulence enhanced cooling as proposed below may enable such gas to cool down and contribute to the observed emission line halos.

An important question is, where the emission line gas is actually located with respect to the structures in the jet simulation. Many authors have assumed that it should be the layer of shocked ambient gas, where the emission line gas actually resides. An alternative location would be the low density jet cocoon (cocoon hereafter). From observations (compare Nesvadba, this volume) the emission line gas is usually volume filling and does not show any kind of shell structure. The latter would be expected if the emission line gas would be located in the shocked ambient gas layer. Therefore, the morphology strongly points to the cocoon as the emission line locus. For an inclination of 70 degree from the jet axis, we have calculated the position velocity diagrams for the cocoon and shocked ambient gas layer, where the two have been separated with a tracer technique (Fig. 1.2). The plot for the shocked ambient gas displays the expected velocities, as they are similar to the sound speed in the ambient gas. However, the approaching and the receding part of the shocked ambient gas layer occupy clearly separated regions, which is usually not observed. A nice feature is the slope of the curve, which might be consistent with the observed large scale velocity gradients. The cocoon gas occupies a coherent region. The velocities here refer to a numerical mixture of relativistic jet and hot entrained ambient plasma. Below, we will show, that the multi-phase turbulence produces a characteristic density velocity relation, which can account for the observed velocities in the emission line gas. A remaining problem for the cocoon locus are the bulk velocities: Cocoons in light jets flow backwards from the hot spots, in the observers frame. Emission line regions are observationally inferred to move outwards. We will address this problem further below.

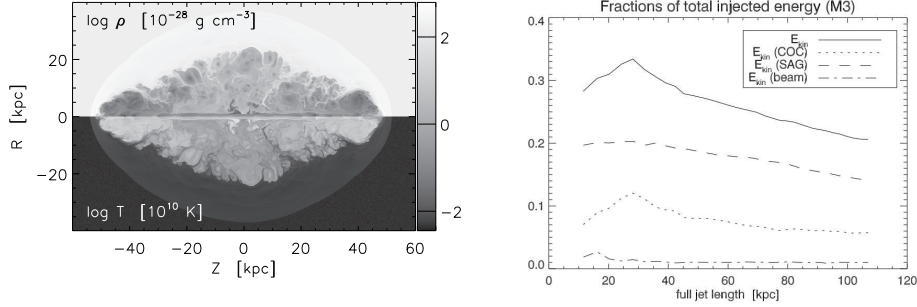


Fig. 1.1. Left: MHD simulation of a very light (density ratio 10^{-3}) jet. Upper part shows the density, lower part the temperature. Right: Kinetic energy as fraction of the total injected energy, for all the simulation and selected regions explained in the text. The remaining energy is thermalised.

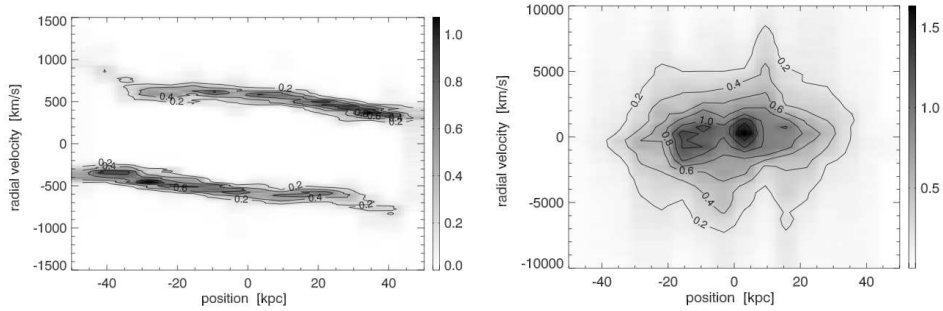


Fig. 1.2. Position velocity diagram for the simulation of Fig. 1.1. Left: Cells in the shocked ambient gas. Right: Cells in the cocoon.

We have calculated the kinetic energy available for cloud acceleration in the two respective regions in question (Fig. 1.1, right). For our reference simulation, the kinetic energy in the cocoon is in the range 5-10 per cent of the total injected energy. For the shocked ambient gas layer, the number is 15-20 per cent. These numbers are anti-correlated with the jet/ambient density ratio. Within the accuracy of the measurements both situations would require a similar conversion between the measured kinetic energy in the emission line regions and the total jet power.

1.3 Local simulations of multi-phase turbulence

The actual emission line gas component cannot be resolved well in global jet simulations. We have therefore done local 3D HD simulations, including

optically thin cooling, also with *NIRVANA*. We simulated essentially the Kelvin-Helmholtz instability with a density ratio of 10,000 and a dense cloud (1 and 10 cm^{-3}) in the middle. The initial Mach number is 0.8 (80) in the hot (intermediate) phase, respectively. In a series of simulations, we vary the cloud density and the temperature of the intermediate (ambient) temperature phase. The cloud is soon disrupted and the non-linear evolution of the instability leads to multi-phase turbulence (Fig. 1.3, left). There are several numerical effects which may play a role here. They are discussed along with more details about the simulations in (18). We believe however that the results we focus on here are not dominated by the numerical issues.

We show a typical temperature histogram in Fig. 1.4 (left). The intermediate temperature gas is still well visible at $5 \times 10^6 \text{ K}$. Numerical mixing produces the flat regions at both sides of this peak. Towards the lower temperature end the cutoff is given by the resolution limit of the simulation. Near 10^4 K , a prominent peak is found. This may be interpreted as shock excited emission line gas. In the following analysis we define gas with a temperature between 10,000 K and 20,000 K as emission line gas.

Fig. 1.3 (right) shows the Mach number - density histogram. The Mach number is not correlated to the density at low densities, where the cooling time is much longer than the simulation time. When cooling is important, the Mach number is proportional to the square root of the density. The result is identical to the 2D case (17). It implies that the velocity distribution of all gas colder than $\approx 10^6 \text{ K}$ should be the same. Also, from the critical density when cooling becomes important down to the density of jet material, the velocity scales with the square root of the density. The velocity of the backflow of the jet plasma in the cocoon should still be of order the speed of light. The critical density is probably not very much higher than the ambient density in these strongly star forming galaxies. The observed width of the emission line gas then requires jet/ambient density ratios of order $10^{-4} - 10^{-3}$, similar to what can be deduced from X-ray observations of sources at low redshift (14; 15).

We show the energy fraction in the emission line gas in Fig. 1.4 (right). Due to the radiative dissipation, the time evolution for each of the different simulations is from high to lower total energy. Except for the highest ambient temperature run, the energy in the emission line gas rises first, and for many simulations levels off at a constant energy. For those simulations, the energy in the emission line gas is a few ten per cent of the total energy. This fraction depends strongly on the mass load, with all the low mass load simulations having a much lower energy fraction in the emission line gas. Our simulations have a mass load of $\approx 10^5 M_{\odot} \text{ kpc}^{-1}$, roughly three orders

of magnitude less than observed extended emission line regions. All this suggests that the latter have most of their turbulent energy in the emission line gas. There could also be a significant fraction in a yet colder component, which our simulations do not resolve well enough.

Our simulations also suggest a relation between the kinetic energy in the emission line gas (far more than the thermal energy in this gas phase) and the radiated power (Fig. 1.5, right). At low kinetic energy, about 10^{12} erg are needed to radiate at 1 erg/s, or equivalently, the radiative dissipation timescale, which is the relevant dissipation timescale for multi-phase turbulence, is 10^{12} s. At higher energy, the dissipation timescale has a wider spread for the different simulations with a tendency to increase to about 10^{13} s. For the observed emission line regions in high redshift radio galaxies, this number is of order 10^{14-15} s, consistent with the observation that the turbulence has just decayed in the larger sources. Again, the kinetic energies we reach in our simulations fall short of the observationally required energies by three to four orders of magnitude, which might well explain the discrepancy in the dissipation timescales.

Finally, we show the time evolution of the cold ($T < 10^6$ K) gas fraction in (Fig. 1.5, right). Depending on the temperature of the intermediate gas, which also determines the total energy in the box, the cold gas fraction is either increasing or decreasing. For about 5 Mio K the initial cold gas fraction of about 95 per cent seems to be right. The result depends on the numerical resolution in the way that we underestimate the cold gas fraction. In summary, for ambient temperatures of up to 5 Mio K, in equilibrium, most of the gas mass should be in the cold phase. From these results, it seems plausible in principle that much of the emission line gas is cooled from entrained warmer ambient gas, with the help of some initial cold gas filaments.

1.4 Discussion and conclusions

We have presented global jet simulations, as well as local box simulations of multi-phase turbulence. Regarding the locus of the emission line gas in high redshift radio galaxies, from the global simulations, both the shocked ambient gas and the radio cocoon have problems. The most severe for the shocked ambient gas is the expected shell morphology and the split nature of the position velocity diagram. While dust may play some role in individual sources, the rarity of these features in observed sources argue against this scenario. The cocoon model requires a detailed model for the multi-phase turbulence in the cocoon. We give such a model with our box simulations,

and show that kinematics and radiated power can be explained. We even can give a possible origin for the emission line gas, namely turbulence enhanced cooling on a small seed cold gas fraction. A remaining problem are the bulk velocities: While the simulations predict inward motion during the active jet phase, the observations, based on the Laing-Garrington-effect, show outflowing gas. Perhaps, a way to make sense of this would be to assume that much of the emission line gas is actually not gas entrained from the halo into the cocoon in a warm phase, but rather initially kinematically cold gas within the galaxy. If the turbulent radio cocoon would interact with a massive gas disk, as those observed at similar redshifts by Foerster Schreiber et al. (7), one would expect a turbulent diffusion into the radio lobes, with about the observed bulk flow properties. This conclusion is supported by a consideration of the momentum in the emission line gas and the jet, respectively. For one bubble of emission line gas the momentum is:

$$P_{\text{elg}} = 10^{51} \text{ g cm s}^{-1} M_{\text{elg},10} v_{\text{elg},500}, \quad (1.1)$$

where $M_{\text{elg},10}$ is the mass of the emission line gas in units of $10^{10} M_{\odot}$ and $v_{\text{elg},500}$ is the bulk outflow velocity in units of 500 km s^{-1} (23). If Cygnus A would be regarded as a prototype for FR II radio sources, then the total mass that has been driven through the jet beam for a ≈ 100 kpc sized source would be of order:

$$M_{\text{jet}} = 10^4 M_{\odot} \dot{M}_{-3} t_7, \quad (1.2)$$

where \dot{M}_{-3} is the jets mass flux in units of $10^{-3} M_{\odot} \text{ yr}^{-1}$, and t_7 is the age of the source in units of 10 Myrs. The total momentum delivered by the jets is hence typically of order

$$P_{\text{jet}} = 10^{48} \text{ g cm s}^{-1} M_{\text{jet},4} \Gamma_3. \quad (1.3)$$

Again, the mass gone through the jet beam is given in convenient units of $10^4 M_{\odot}$ and the jets bulk Lorentz factor was scaled to three. So, unless the jets are extremely relativistic, which seems unlikely, the jet's momentum falls short of the one required to accelerate the emission line gas by orders of magnitude. So, while the jet energy is enough to cause turbulent motion, the momentum is too small to be responsible for the directed motions. Further support for this scenario comes from the HI shells surrounding small high redshift radio galaxies, only (16). They have a typical diameter of 50 kpc, and a typical velocity of 200-300 km/s. The energy required to drive these shells can therefore be precisely calculated and is of order one supernova per year, corresponding to star formation rates in excess of $100 M_{\odot} \text{ yr}^{-1}$. This is actually found in observations (7). If this is hence indeed evidence for the

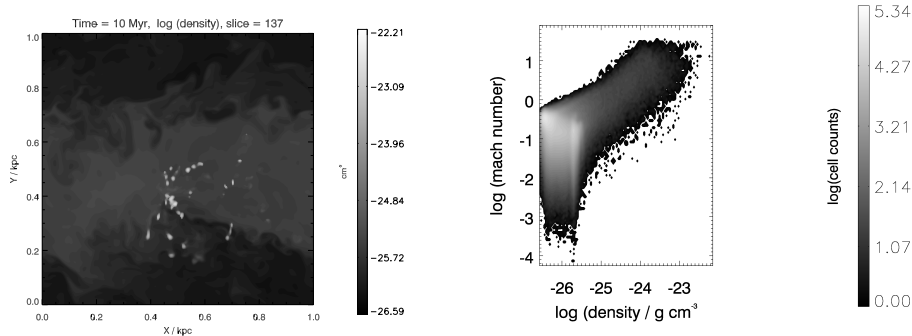


Fig. 1.3. Left: Density slice through the μ 1T5HR (see caption of Fig. 1.5, for a description of the numbers) simulation at 10 Myr. Right: Mach number density histogram for the same simulation.

finishing of a starburst, one could interpret the emission line halos as the missing observational evidence for the late phase in galaxy merger simulations with active black holes (6): Due to the shape of the cavities drilled by the jets, the expelled gas is not distributed isotropically, but aligned with the radio jets.

What happens to the gas, when the active jet phase terminates? We have carried out simulations of the long term effect of radio sources representing the emission line gas by tracer particles (12). Powerful jets set up a long term gas convection that may persist for many Gyrs. From these simulations, we predict the emission line gas to be distributed in the ambient gas, contributing to the halo metallicity.

Focusing again on the black hole, the emission line regions give power estimates close to the emitted radio power. Together they approach 10^{46} erg/s. The jets must have considerably more than this to keep propagating. We showed above that overall of order 1 per cent, maybe up to 10 per cent of the total jet energy should be expected to appear as kinetic energy in the emission line gas. Hence, extended emission line regions point to kinetic jet powers of order 10^{47} erg/s or greater. This is of order the Eddington power for a $10^9 M_{\odot}$ black hole. If the accretion state of the central quasar could be sufficiently constrained, one might be able to infer, whether the jet is powered by accretion directly or by the spinning down of the central black hole.

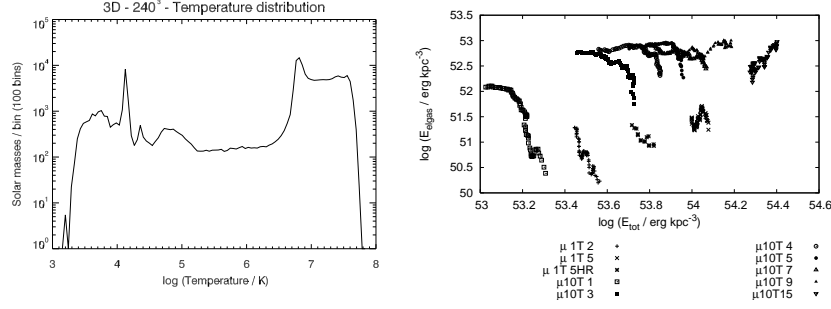


Fig. 1.4. Left: Temperature histogram ($\mu 1T5HR$). Shock excitation and cooling together produce the pronounced peak at 10^4 K, here identified with the emission line gas. Right: Energy in the emission line gas versus total energy in the simulation. The simulations with low mass load have a lower fraction of their energy in the emission line gas. The time evolution is from high total energy to lower total energy.

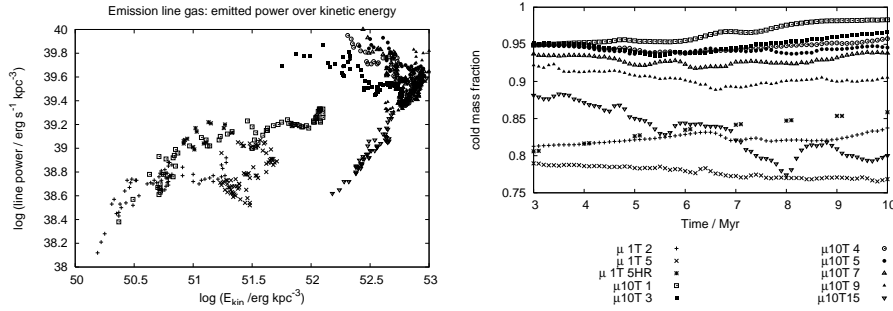


Fig. 1.5. Left: Radiative power, emitted by the emission line gas (temperature in the range from 10,000 K to 20,000 K) over Kinetic energy of this gas. Different symbols are used for different runs shown at many times, as indicated in the legend. μxTy denotes an initial cloud density of $x m_p \text{ cm}^{-3}$ and an initial temperature of the intermediate component of y Mio. K. Right: Cold gas ($T < 10^6$ K) fraction over time.

References

- [1] Best, P. N., Longair, M. S., & Rottgering, H. J. A. (1996). Evolution of the aligned structures in $z \approx 1$ radio galaxies, *MNRAS* **280**, L9
- [2] Bîrzan, L., McNamara, B. R., Nulsen, P. E. J., Carilli, C. L., & Wise, M. W. (2008). Radiative Efficiency and Content of Extragalactic Radio Sources: Toward a Universal Scaling Relation between Jet Power and Radio Power, *ApJ* **686**, 859
- [3] Blandford, R. D., & Znajek, R. L. (1977). Electromagnetic extraction of energy from Kerr black holes, *MNRAS* **179**, 433
- [4] Camenzind, M. (1991). Magnetohydrodynamics of Black Holes and the Origin of Jets, *New York Academy Sciences Annals* **647**, 610
- [5] Dey, A., van Breugel, W., Vacca, W. D., & Antonucci, R. (1997). Triggered Star Formation in a Massive Galaxy at $Z = 3.8$: 4C 41.17, *ApJ* **490**, 698
- [6] Di Matteo, T., Springel, V., & Hernquist, L. (2005). Energy input from quasars regulates the growth and activity of black holes and their host galaxies, *Nature* **433**, 604
- [7] Forster Schreiber, N. M., et al. (2009). The SINS survey: SINFONI Integral Field Spectroscopy of $z \approx 2$ Star-forming Galaxies, *arXiv* **0903.1872**
- [8] Gaibler, V., Camenzind, M., & Krause, M. (2008). Large-Scale Propagation of Very Light Jets in Galaxy Clusters in *Extragalactic Jets: Theory and Observation from Radio to Gamma Ray*, ASP conference series (San Francisco) **386**, 32
- [9] Gaibler, V., Krause, M., & Camenzind, M. (2009). Very light magnetized jets on large scales - I. Evolution and magnetic fields *MNRAS*, submitted
- [10] Häring, N., & Rix, H.-W. (2004) *ApJ Letter* **604**, 89
- [11] Hawley, J. F., Beckwith, K., & Krolik, J. H. (2007). General relativistic MHD simulations of black hole accretion disks and jets, *Ap&SS* **311**, 117
- [12] Heath, D., Krause, M., & Alexander, P. (2007). Chemical enrichment of the intracluster medium by FR II radio sources, *MNRAS* **374**, 787
- [13] Krause, M., & Camenzind, M. (2003). Parameters for very light jets of cD galaxies *New Astronomy Review* **47**, 573
- [14] Krause, M. (2003). Very light jets. I. Axisymmetric parameter study and analytic approximation *A&A* **398**, 113
- [15] Krause, M. (2005). Very light jets II: Bipolar large scale simulations in King atmospheres, *A&A* **431**, 45
- [16] Krause, M. (2005). Galactic wind shells and high redshift radio galaxies. On the

- nature of associated absorbers, *A&A* **436**, 845
- [17] Krause, M., & Alexander, P. 2007. Simulations of multiphase turbulence in jet cocoons, *MNRAS* **376**, 465
- [18] Krause, M. G. H. (2008). Jets and multi-phase turbulence, *Memorie della Societa Astronomica Italiana* **79**, 1162
- [19] McCarthy, P. J. (1993). High redshift radio galaxies, *A&A Review*, **31**, 639
- [20] McNamara, B. R., Kazemzadeh, F., Rafferty, D. A., Bîrzan, L., Nulsen, P. E. J., Kirkpatrick, C. C., Wise, M. W. (2009). An Energetic AGN Outburst Powered by a Rapidly Spinning Supermassive Black Hole or an Accreting Ultramassive Black Hole, *ApJ* **698**, 594-605
- [21] Miley, G., & De Breuck, C. (2008). Distant radio galaxies and their environments, *A&A Review* **15**, 67
- [22] Müller, A., & Camenzind, M. (2004). Relativistic emission lines from accreting black holes. The effect of disk truncation on line profiles, *A&A* **413**, 861
- [23] Nesvadba, N. P. H., Lehnert, M. D., De Breuck, C., Gilbert, A. M., van Breugel, W. (2008). Evidence for powerful AGN winds at high redshift: dynamics of galactic outflows in radio galaxies during the “Quasar Era”, *A&A* **491**, 407-424
- [24] Nulsen, P. E. J., Hambrick, D. C., McNamara, B. R., Rafferty, D., Birzan, L., Wise, M. W., & David, L. P. (2005). The Powerful Outburst in Hercules A, *ApJ Letter* **625**, L9
- [25] Tortora, C., Antonuccio-Delogu, V., Kaviraj, S., Silk, J., Romeo, A. D., & Becciani, U. (2009). AGN jet-induced feedback in galaxies - II. Galaxy colours from a multcloud simulation, *MNRAS*, **630**
- [26] Young, A. J., Lee, J. C., Fabian, A. C., Reynolds, C. S., Gibson, R. R., & Canizares, C. R. (2005). A Chandra HETGS Spectral Study of the Iron K Bandpass in MCG -6-30-15: A Narrow View of the Broad Iron Line, *ApJ* **631**, 733
- [27] Ziegler, U., & Yorke, H. W. (1997). A nested grid refinement technique for magnetohydrodynamical flows, *Computer Physics Communications* **101**, 54